Surface Science 605 (2011) 483–488

Contents lists available at ScienceDirect

Surface Science

journal homepage: www.elsevier.com/ locate/susc

Structures of AgPd nanoclusters adsorbed on MgO(100): A computational study

Fabio R. Negreiros [a,b,c], Giovanni Barcaro [c], Zdenka Kuntová [b,d], Giulia Rossi [b,e], Riccardo Ferrando [b,*], Alessandro Fortunelli [c]

[a] Depto. de Física, ICEx, Universidade Federal de Minas Gerais, CP702, Belo Horizonte, MG, Brazil
[b] Dipartimento di Fisica and CNISM, Via Dodecaneso 33, Genova, I16146, Italy
[c] Molecular Modeling Laboratory, IPCF/CNR, via G. Moruzzi 1, Pisa, I56124, Italy
[d] Institute of Physics, AS CR, v.v.i., Na Slovance 2, 182 21 Prague 8, Czech Republic
[e] Department of Applied Physics, Aalto University, P.O.Box 1100 FI-00076 Aalto, Finland

ARTICLE INFO

Article history:
Received 23 October 2010
Accepted 2 December 2010
Available online 10 December 2010

Keywords:
Density functional calculations
Monte Carlo simulations
Clusters
Palladium
Silver
Magnesium oxides

ABSTRACT

The structures of AgPd clusters supported on MgO(100) are investigated via a combination of global optimization searches within an atom–atom potential model and density-functional calculations. Although pure Ag and Pd clusters favor fcc structures in (100) epitaxy with the substrate, it is found that AgPd mixing creates a pocket of stability for polyicosahedral structures in the AgPd/MgO(001) nanoalloy phase diagram. Polyicosahedra are very stable for size around 40 atoms, where they compete with fcc(100) and decahedral structures. For clusters with up to 200 atoms and 50%–50% composition, these last two structural motifs are the most stable ones at the atom–atom potential level. For sizes of 400 atoms, fcc structures in (111) epitaxy with the substrate become close in energy to fcc(100) and Dh clusters, indicating a likely transition to (111) epitaxy for larger sizes.

1. Introduction

Alloy nanoparticles (or nanoalloys) [1] are bi- or multi-component nanoparticles of atomic elements that are metals in their bulk form. These systems are of great interest from the experimental, theoretical and modelling point of views, with applications ranging from catalysis, to optics and magnetism. In particular, silver–palladium nanoalloys have been recently studied because of their applications in hydrogenation reactions with enhanced selectivity [2,3].

In a previous paper [4], the structures of gas-phase AgPd nanoalloys were computationally studied by an approach [5] combining global optimization searches within an empirical potential (EP) model together with density-functional (DF) local relaxation of selected isomers belonging to the significant structural families. An improved EP for the Ag–Pd binary system was derived and it was shown that it provides a fairly accurate description of AgPd nanoclusters in the gas phase, especially for sizes large enough (from 100 atoms on). In particular, in Ref. [4] it was shown that the stability of polyicosahedral structures [6], originally proposed as the global minima of gas-phase AgPd clusters [7], is not fully confirmed by a more accurate representation of metal–metal interactions.

Here we focus on the determination of the structures of AgPd nanoalloys supported on MgO(100). This substrate is one of the most widely studied supports for model catalysts [8,9]. The MgO(100) face exposes a checkerboard of alternating oxygen and magnesium atoms. Pd and Ag atoms adsorb preferentially on top of oxygen [10–22]. While pure Ag and Pd clusters on MgO(100) have been widely studied both experimentally [8,9,15,23] and computationally [19,21,22,24–30], much less is known about AgPd nanoalloys on the same support. AgPd nanoparticles have been produced by vapor deposition onto thin alumina films [31]. These particles were identified as presenting an intermixed chemical ordering but with some silver segregating at the surface. Theoretical studies are limited to very small sizes, which nevertheless suggest that AgPd mixing has an appreciable effect on both structural an electronic properties [32]. It should be noted that we focus here on the pristine, undefected MgO(100) surface. Surface hydroxylation can however be expected in non-ultra-high-vacuum conditions affecting epitaxial phenomena. Moreover, even though the effect of point defects [32] is likely to be weakened for medium-sized clusters such as those here investigated, the presence of extended defects (such as steps) can be important (and has been invoked [22])) in orienting the cluster morphology.

Experiments and simulations have shown that pure Ag and Pd clusters on MgO(100) mostly grow in cube-on-cube epitaxy with the substrate. In this case, the metals adhere to the substrate by (100) facets, starting from very small sizes (~10–15 atoms for Pd [30]). This epitaxy will be indicated hereafter as fcc(100) epitaxy. Another epitaxy is possible, in which the metals adhere with (111) facets, but it was found to be much less frequent for both pure Ag and Pd.

As shown in the following, the case of AgPd nanoalloys presents a much richer phenomenology. Even though the substrate is of square symmetry, its effect is of stabilizing, for some sizes and compositions,

* Corresponding author. Fax: +39 010314218.
E-mail address: ferrando@fisica.unige.it (R. Ferrando).

0039-6028/$ – see front matter © 2010 Elsevier B.V. All rights reserved.
doi:10.1016/j.susc.2010.12.002

six-fold polyicosahedral structures, that are not the most favourable in the gas phase but surprisingly become the lowest in energy due to the contact with the substrate. In fact, Ag–Pd mixing creates a pocket of stability for polyicosahedral structures in the Ag–Pd supported nanoalloy phase diagram. These structures are stable both at the EP and DF level around 40-atom size, competing with (100) and decahedral (Dh) motifs. For somewhat larger clusters, polyicosahedral structures become less competitive, while fcc(100) and Dh motifs become the most stable ones, in close competition up to size 200 atoms at least. For even larger sizes, fcc structures in fcc(111) epitaxy with the substrate may become competitive and eventually dominate the structural landscape.

Ag and Pd are fully miscible in the bulk phase, but without evidence of the formation of ordered phases [33]. As we will see, nanoscale effects will induce specific features in the chemical ordering, due both to the metal–metal interaction in the vicinity of the free cluster surfaces, and to the metal–substrate interaction at the interface with MgO.

The article is structured as follows. In Section 2 we sketch the EP model and the computational methodology. Section 3 is devoted to the results. We consider sizes $N=40$, 60, 100, 200 and 400. In particular, for size 40, compositions $Ag_{10}Pd_{30}$, $Ag_{20}Pd_{20}$ and $Ag_{30}Pd_{10}$ are considered. For size 60 and beyond, we focus only on the 50% composition, what is sufficient to provide the structural phase diagram of the mixed Ag–Pd alloy and the chemical ordering variation with size. Section 4 contains the conclusions.

2. The approach

2.1. The empirical potential (EP)

For the determination of the energy of Ag–Pd supported particles, a combination of EPs based on the second-moment approximation to the tight–binding theory for the metal–metal binding [34–36] and a many-body EP assuming a rigid metal–oxide potential energy surface for the metal–substrate interaction [19] was used. The total binding energy E_{bnd} of a cluster of N atoms is then written as the sum of atomic contributions E_i, distinguished into metal–metal energy contributions (E_i^{mm}) and the metal–oxide interaction (E_i^{mo}):

$$E_{bnd} = \sum_{i=1}^{N} E_i, \tag{1}$$

with

$$E_i = E_i^{mm} + E_i^{mo}, \tag{2}$$

E_i^{mm} is defined as:

$$E_i^{mm} = E_i^r + E_i^a \tag{3}$$

with

$$E_i^r = \sum_{i\neq j}^{N} A(a,b)e^{-p(a,b)\left(r_{ij}/r_0(a,b)-1\right)} \tag{4}$$

$$E_i^a = \left[\sum_{i\neq j}^{N} \xi^2(a,b)e^{-2q(a,b)\left(r_{ij}/r_0(a,b)-1\right)}\right]^{1/2} \tag{5}$$

where $a(b)$ represents the atomic species of atom i (j), r_{ij} is the distance between these atoms, r_c is the cutoff radius, and r_0, ξ, q, p and A are adjustable parameters. The potential is smoothly linked to zero by a polynomial function, between third- and fourth-neighbour distances (the cutoff radius r_c). The parameter sets $\{A,\xi,p,q,r_0\}$ used in the present work differ from the ones previously employed in the literature [7,37–39] and are taken from Ref. [4] to which we refer for a detailed discussion.

E_i^{mo} is defined as:

$$\begin{aligned} E_i^{mo}(x_i,y_i,z_i,Z_i) &= a_1(x_i,y_i,Z_i)\left\{e^{-2a_2(x_i,y_i,Z_i)[z_i-a_3(x_i,y_i,Z_i)]} - 2e^{-a_2(x_i,y_i,Z_i)[z_i-a_3(x_i,y_i,Z_i)]}\right\},\\ a_j(x_i,y_i,Z_i) &= b_{j1}(x_i,y_i) + b_{j2}(x_i,y_i)e^{-Z_i/b_{j3}(x_i,y_i)}\\ b_{jk}(x_i,y_i) &= c_{jk1} + c_{jk2}\{cos(\chi x_i) + cos(\chi y_i)\} +\\ &\quad + c_{jk3}\{cos(\chi(x_i+y_i)) + cos(\chi(x_i-y_i))\} \end{aligned} \tag{6}$$

where Z_i is the number of metal nearest neighbors of atom i, and $\chi=2\pi/a$, with a the oxygen–oxygen distance in the substrate. The x and y coordinates are parallel to the <110> directions. Z_i is calculated including all neighbours within 1.25 r_0, with r_0 the nearest neighbour distance in the bulk metal. Eq. (6) contains 27 parameters c_{jkl}. Those for Pd were taken from the original work [19], and produce results in reasonable agreement with DF calculations [30] for clusters of sizes up to 30 atoms. Those for Ag were fitted in Ref. [21] to take into account the "metal-on-top" effect [40], i.e., the enhancement in the adhesion energy due to the stabilizing contribution of metal atoms above the one directly interacting with the substrate, via a proper choice of the fitting systems. The parameters c_{jkl} in Eq. (6) can be found on the Web [41].

2.2. The basin-hopping algorithm

The search for the best motifs and the best homotops was performed using a basin-hopping (BH) algorithm [42–44]. BH combines a Metropolis Monte Carlo approach with local minimization of the sampled configurations. For each size and composition, at least four Monte Carlo (MC) runs were performed using a number of steps of the order of 10^5. Three different order parameters were used in order to increase the structural diversity in the output: the (5,5,5) signature of the common neighbor analysis (CNA) [45]; the number of metal atoms in contact with the MgO(100) surface; the total number of mixed bonds. In each step, either a shake move, that consists in displacing all atoms from their original position in a random direction by up to 1.5 Å, or a Brownian move (a Molecular-Dynamics run at 3000 K) was adopted. The acceptance of each move depended on the temperature and the methodology, that can be one of the three following cases:

a) A standard MC Metropolis algorithm, with simple shake moves and temperatures varying from 2000 to 5000 K for clusters up to 200 atoms, or Brownian moves and temperatures varying from 500 to 1000 K for clusters of 200 or 400 atoms;
b) A MC algorithm that takes into account the memory of previously obtained structures [44], favoring the ones that have a different order parameter. When a transition from state A to state B is attempted, a perturbation term equal to $w(h_A-h_B)$ is added to the energy of the MC acceptance rule, where h_A (h_B) is the percentage of structures obtained in the previous part of the simulation with a CNA parameter equal to A (B) and w is a weight, chosen as $w=10$ eV in our calculations. The temperature varies from 500 to 3000 K.
c) A parallel excitable walkers [43,44] algorithm, in which a set of random initial configurations, named as walkers, follow a regular MC run under the constraint that there is an additive energy term to the MC acceptance rule to avoid the same order parameter of two or more walkers. In this work 5 walkers were used and the repulsive energy was chosen equal 0.7 eV. The temperature varies from 100 to 1000 K.

As a final step, once a large set of low energy structures are found, a search for the best homotop within each motif is performed via an exchange-only basin-hopping algorithm [46] allowing at each iteration a single atom–atom exchange at a low temperature (between 100 K and 200 K) with a number of steps varying between 10,000 and 100,000, depending on the total number of atoms of the cluster.

2.3. Density functional calculations

The DF calculations were performed with the plane-wave-based Quantum Espresso package [47] that solves the Kohn–Sham equations using the generalized-gradient exchange-correlation functional approximation (GGA) proposed by Perdew, Burke and Ernzerhof [48] and ultrasoft pseudopotentials [49]. An energy cutoff of 550 eV for the wave functions was used, and eigenvalues and eigenvectors of the Kohn–Sham Hamiltonian were evaluated at the Γ point, having verified that this approximation does not appreciably influence the accuracy of the results. The size of the cubic cell containing the clusters was large enough to guarantee that the distance between the closest atoms among neighbor images was never lower than 7.5 Å, in all directions, and two fixed layers of MgO(100) were used in order to reproduce the oxide substrate. Earlier work [30] has shown that the relaxation of the MgO surface due to the metal adsorption is quite weak and can be neglected. Geometry relaxations were performed by optimizing the position of all atoms until the forces were less than 0.03 eV/Å. All the calculations were performed spin unrestricted.

3. Results and discussion

In the following, the results of the EP simulations at size 40, 60, 100 and 200 atoms are presented. We separate size 40, at which we compare DF and EP results in order to double-check the accuracy of the EP, and larger sizes, for which only EP results will be reported. It has been shown in fact [4] that the EP predictions on the energetics of AgPd clusters are more and more accurate as the size of the clusters increases beyond 80 atoms.

3.1. 40-atom clusters

Fig. 1 shows most of the different isomers obtained in this work at composition 50%. Dh structures, such as Dh_1, Dh_2 and Dh_3, correspond to different (incomplete) decahedra, while Ih represent icosahedra. Among poly-icosahedral (pIh) structures, the six-fold pIh (or "pancake", pc6) occurs most frequently. It achieves shell closure at size 38 atoms: $pc6_1$ and $pc6_2$ correspond to two different ways of arranging two additional atoms on the perfect 38-atom pc6. $fcc(100)_2$, $fcc(100)_2$ and $fcc(100)_3$ are fcc(100) stackings that expose different number of 5-fold and 6-fold faces. Finally, $fcc(100)_{Ag}$ and $fcc(100)_{Pd}$ corresponds to the best fcc(100) structure for pure Ag and Pd, respectively, while fcc(111) adheres to the substrate with a (111) facet.

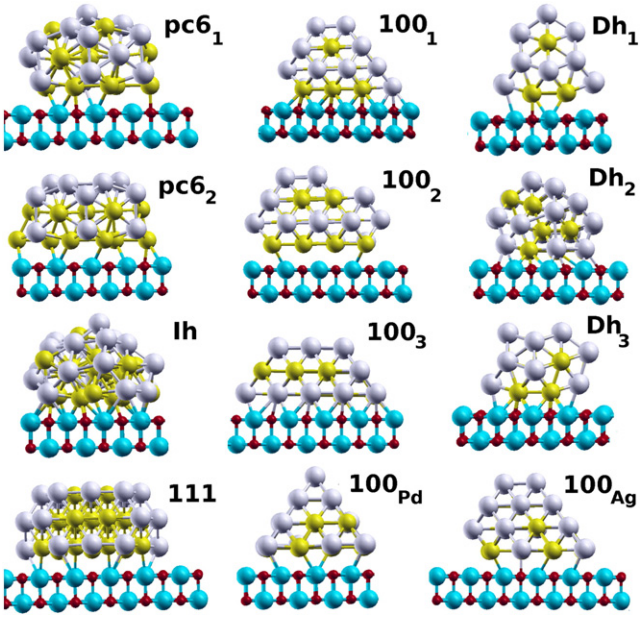

Fig. 1. The main structural motifs of 40-atom clusters at composition 50% are shown. Ag, Pd, Mg and O atoms are in grey, yellow, blue and red, respectively. Some small variations on each image occurs for the other concentrations specified in Table 1. The motif $fcc(100)_1$ is very similar to $fcc(100)_{Ag}$ and was not shown in this plot. (For interpretation of the references to colour in this figure legend, the reader is referred to the web version of this article.)

The relative energy of each structure is reported in Table 1. As it can be seen, the performance of the EP is fairly good, especially at 50%–50% composition, and the predicted energy differences are only 0.1–0.5 eV off DF values. A comparison with previously used EPs [7,37–39] (not reported here) also shows that the current EP provides not only a better agreement but a better set of motifs at the DF level. The most notable results that can be derived from an inspection of Table 1 is that at composition 50% the most stable structure at both the EP and DF levels is the pc6. Given that this motif is not competitive for the pure counterparts, its low energy can only be understood by a stabilization of the mixed Ag–Pd bonds, which optimizes the metallic energy of the nanocluster. On the opposite, the fcc(100) motif has a good epitaxial match with the substrate, thus maximizing the number of Pd–O bonds and increasing the metal–oxide interaction. The Dh motif can be considered as intermediate between these two extremes, combining a reasonably good epitaxial stacking with some internal strain. Last, the fcc(111) motif represents a very good and unstrained crystalline structure at the cost of a non-epitaxial growth on the substrate.

For compositions other than 50%, i.e., 25–75% and 75–25%, the energy of the best motifs obtained at the EP level are shown in Table 1. Again, a fairly good agreement with DF predictions is obtained, and it can be noted that pIh structures are still favored by the Ag–Pd mixing. Thus, these motifs are stable for a large concentration range and should be, according to EP and DF predictions, at least as common as other motifs around this size.

As noted for free Ag–Pd clusters [4], the Pd atoms preferentially occupy high-coordinated sites on Ag–Pd nanoclusters, such as in the core or in the center of the (111) faces. At the same time, the Pd–O bond is stronger than the Ag–O bond, so that the nanoalloy/MgO interface may be expected to consist of Pd atoms on top of O atoms. In order to check which is the best chemical ordering of supported Ag–Pd clusters, Table 2 shows the energy of 7 homotops of a 40-atom $Ag_{30}Pd_{10}$ fcc(100) motif at the EP and DF level together with the number of Pd atoms on the center of (111) faces (N_{111}) and on top of oxygen(N_S). First, it is worth noticing that a good agreement between EP-DF is again obtained. Second and most important, EP and DF calculations agree that the best homotops have a balanced amount of Pd splitted between surface and interface sites. This remains true for other concentrations and other motifs, so it is a general trend at this size.

Table 1
For 40-atom AgPd clusters supported on MgO(100) at 25, 50% and 75% composition, the energy (in eV) of the lowest energetic motifs obtained at the EP and DF level are shown. Refer to Fig. 1 for an image of the motifs at 50% composition.

$Ag_{10}Pd_{30}$			$Ag_{20}Pd_{20}$			$Ag_{30}Pd_{10}$		
Motif	EP	DF	Motif	EP	DF	Motif	EP	DF
$fcc(100)_{Ag}$	0.00	0.00	$pc6_1$	0.00	0.00	Dh_3	0.43	0.00
$pc6_1$	0.50	0.06	Dh_1	0.26	0.28	Ih	0.28	0.05
$fcc(100)_2$	0.44	0.29	$fcc(100)_1$	0.43	0.30	$pc6_1$	0.00	0.12
fcc(111)	0.13	0.62	$fcc(100)_{Ag}$	0.65	0.34	$fcc(100)_{Ag}$	0.57	0.20
Dh_2	0.25	0.65	$fcc(100)_2$	0.51	0.37	fcc(111)	0.30	0.39
Dh_1	0.31	0.87	fcc(111)	0.32	0.42	fcc(100)	0.91	0.51
Ih	0.40	0.84	$pc6_2$	0.78	0.66	$pc6_2$	0.39	0.56
			$fcc(100)_3$	1.43	1.31			
			$fcc(100)_{Pd}$	2.36	2.34			

Table 2
The energy differences (in eV) with respect to the lowest energy homotop for 40-atom clusters belonging to the fcc(100)$_{Ag}$ motif and supported on MgO(100) at composition $Ag_{30}Pd_{10}$ are shown at the EP and DF level. The number of Pd atoms on (111) sites (N_{111}) and in contact with the MgO(100) surface (N_S) are also shown for each homotop. The total number of atoms in contact with the surface is 14.

Homotop	N_{111}	N_S	EP	DF
1	2	4	0.00	0.00
2	2	3	0.06	0.00
3	1	4	0.07	0.11
4	2	3	0.29	0.14
5	3	2	0.21	0.18
6	0	5	0.04	0.29
7	0	6	0.36	0.57

3.2. Clusters with 60, 100, 200, and 400 atoms

As the EP potential is expected to assure a progressively better agreement with DF calculations as the size of the cluster increases to 100 atoms and beyond [4], only EP simulations were performed on the larger Ag–Pd clusters deposited on MgO(100). Attention will be focused on two points: the size range in which each structural motif represents the most stable one, and the patterns of chemical ordering as a function of the cluster size. Only 50%–50% composition will be considered.

3.2.1. The low-energy structures

The relative energies of the most representative motifs with 60, 100 and 200 atoms at the EP level are reported in Table 3, and are shown in Fig. 2 for size 100 and 200 atoms. Note that only a small selection of the obtained structures is reported, with the goal of describing the crossover among motifs rather than analyzing fine details of each structural family. For all the sizes here considered, the lowest-energy isomers were found to be fcc(100) and Dh structures. These two motifs lie very close in energy in the entire size range, and no indications of a clear crossover can be observed. Ih and pIh structures are less and less competitive as the cluster size increases, and for 200 atoms they lie above the putative global minimum by more than 2 eV. fcc(111) motifs, show some decrease of their energy difference with respect to Dh and (100) motifs.

For size 400 (see Fig. 3), the three structural motifs are quite close in energy. The Dh structure is quasi-degenerate with the fcc(100) structure, which is higher by 0.06 eV. The fcc(111) motifs is somewhat less favourable, but not much higher in energy (0.65 eV).

AgPd clusters thus present some clear differences compared to pure Ag and Pd clusters on MgO. In fact, for AgPd clusters at 50% composition, Dh structures are closely competing with fcc(100) structures, a behavior which is not found for single-component nanoparticles. For $N=100$, Dh structures are the lowest in energy, at variance with both Ag and Pd pure clusters [21,22]. The transition from fcc(100) to fcc(111) epitaxy is not taking place up to $N=400$, even though fcc(111) clusters begin to be competitive at this size. This is consistent with the results of this model for pure clusters, which locates this transition at $N\simeq 700$ for pure Pd and above 3000 atoms for pure Ag [21,22].

Table 3
Energies (in eV) relative to the putative global minimum are reported for the most representative Ag–Pd clusters supported on MgO(100) with 60, 100 and 200 atoms and at 50% composition, as obtained at the EP level. In Fig. 2 some of these motifs are shown.

60 atoms		100 atoms		200 atoms		400 atoms	
Motif	EP	Motif	EP	Motif	EP	Motif	EP
fcc(100)	0.00	Dh	0.00	fcc(100)	0.00	Dh	0.00
Dh	+0.23	fcc(100)	+0.15	Dh	+0.94	fcc(100)	+0.06
Ih	+0.79	fcc(111)	+0.92	fcc(111)	+1.02	fcc(111)	+0.65
pc6-cov	+1.28	Ih-AM	+1.47	Ih	+3.31		
fcc(111)	+1.71						

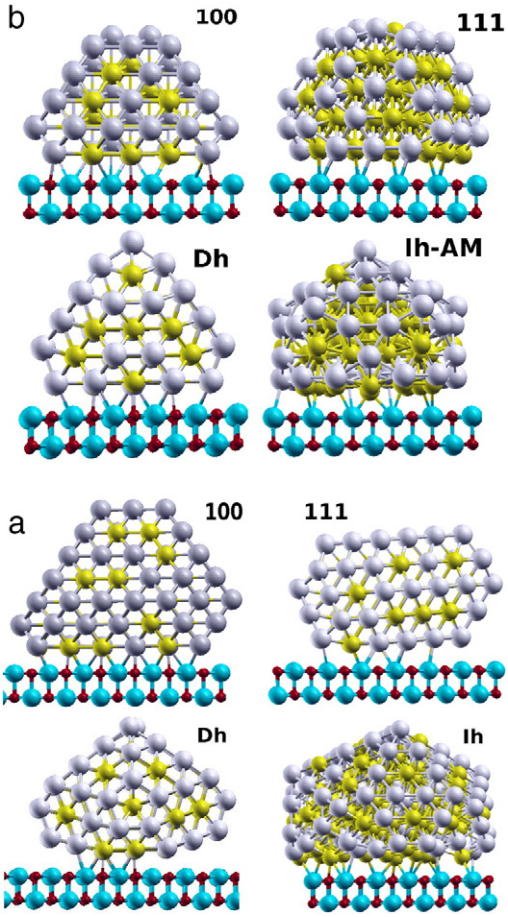

Fig. 2. The main structural motifs obtained at size 100 (b) and 200 (a) atoms and composition 50% are shown. The energy of each motif is reported in Table 3. Symbols as in Fig. 1.

3.2.2. Patterns in Ag–Pd chemical ordering

Fig. 4 shows the radial distributions of Ag and Pd as a function of the distance from the center of the cluster for fcc(100)-type structures at different sizes and 50% composition. At size 60, it can be seen that Pd is mostly located in the subsurface shell, and populates almost exclusively also the inner core and the centers of the (111) facets (a clear sign of the latter is the outmost peak at 6 Å in the Pd radial distribution). Ag, instead, is predominantly located at the surface, with minor population of the inner core and the second shell. Entering the cluster from one of its free surfaces, three-shell arrangement is thus encountered: silver-rich outer layer, palladium-rich subsurface layer and intermixed particle core. This is in reasonable agreement with the growth structures obtained by previous molecular-dynamics simulations on gas-phase clusters [50], with the proviso, however, that both first and second shell are populated by both species. On the other hand, the interface layer in contact with the substrate is enriched in Pd. For sizes 100 and 200, a similar pattern is found, although the tendency of Pd to subsurface segregation and in general the driving force to multi-shell arrangements is weaker, and there are signs of random alloy formation especially in the core of the cluster as the size increases. A decreased driving force to multi-shell arrangements as the cluster size increases is to be expected on general grounds [1], and is here enhanced by the geometrical frustration due to the cluster/substrate interaction.

An interesting observation in this connection is in fact that the number of Ag atoms at the nanocluster/substrate interface progressively increases with size in fcc(100) structures: the fraction of Ag atoms at the interface is 39%, 44% and 48% for sizes 100, 200 and 400, respectively. Analyzing the relative positions of Ag and Pd atoms in more detail, one can note that a chess-board pattern (i.e., a square pattern alternating Ag

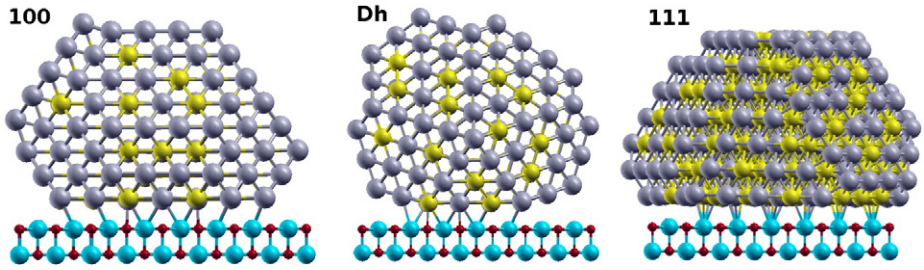

Fig. 3. Main structural motifs obtained at size 400 and composition 50%. Symbols as in Fig. 1

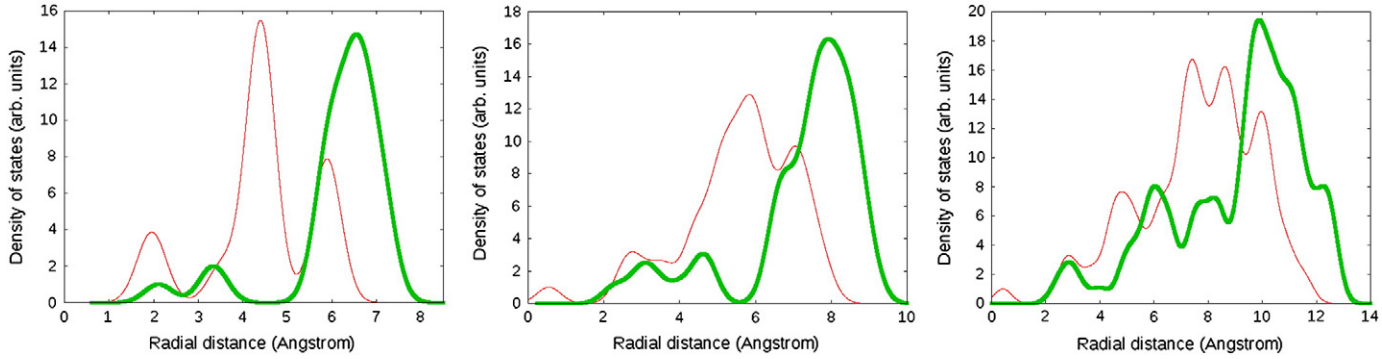

Fig. 4. Ag (thick line) and Pd (thin line) radial distributions as a function of the distance from the center of the fcc(100) cluster for 60-atom (left), 100-atom (middle) and 200-atom (right) particles. The height of the center of the cluster is taken at 2.5 Å above the MgO(100) surface.

and Pd atoms) is progressively formed, with nearly half sites being occupied by Ag atoms. We note that a presence of Ag atoms at the interface helps in releasing the strain associated with the mismatch between Pd and the substrate. The lattice mismatch between Pd and O–O distance in MgO is of 7.6%. As the cluster size increases, the strain causes a decrease of the adhesion energy per unit area of pure Pd clusters in fcc(100) epitaxy [22]. On the contrary, the adhesion energy of pure Ag clusters changes weakly, because of the smaller mismatch (3%). In mixed clusters, the insertion of some Ag atoms at the interface relatively improves the adhesion energy. Moreover, as the size of the cluster increases, the metal–surface interaction becomes less important because of the increased metal coordination and the decreased relative weight of the interface, so that the metal–metal energetics finally tends to prevail over the metal–oxide one. This in turn translates into a tendency to maximizing the number Ag–Pd bonds and equalizing the number of Pd–O and Ag–O bonds.

4. Conclusions

Although pure Ag and Pd clusters favor fcc(100) motifs when grown on MgO(100), it is found that Ag–Pd mixing creates a pocket of stability for polyicosahedral motifs in the Ag–Pd supported nanoalloy phase diagram. This structure is very stable at the EP and DF level at 40-atom size, competing with fcc(100) and Dh motifs. We recall that in gas-phase clusters, the sixfold polyicosahedral motifs is unfavorable at the DF level [4]. Therefore the square-symmetry substrate has the quite surprising effect of stabilizing this structure.

For larger sizes, we have considered only 50%–50% compositions. For clusters with up to 200 atoms, these last two structures are the most stable ones at the EP level, with Dh clusters prevailing for size 100 and fcc(100) clusters prevailing for size 200. This is a remarkable difference with respect to both pure Ag and Pd clusters, in which Dh structures are always much higher in energy than fcc(100) ones. For size 400 atoms, Dh and fcc(100) are almost degenerate, and also fcc (111) structures are in rather close competition, indicating the possible approach to a crossover between epitaxies, which however still remains an open issue. Ordering patterns in AgPd nanoparticles show a three-shell arrangement, with a surface shell (of monoatomic thickness) which is Ag-rich, followed by a Pd-rich subsurface shell and by an intermixed core. The tendency to this three-shell arrangement is however hindered by the interaction with the substrate which causes a Pd-enrichment at the bottom interface.

Acknowledgments

FRN is grateful to the Brazilian CNPq funding agency for financial support. AF acknowledges financial support from the ERC-AG SEPON project (EC VII FP, contract number ERC-2008-AdG-227457). RF acknowledges support from Italian MIUR for the PRIN project 2007LN873M 003. Part of the DF calculations were performed at CASPUR Supercomputing Center (Rome, Italy) within the “Competitive HPC Grant 2009” E-MOON project. The authors acknowledge the support from the COST Action MP0903 Nanoalloys as Advanced Materials: From Structure to Properties and Applications.

References

[1] R. Ferrando, J. Jellinek, R.L. Johnston, Chem. Rev. 108 (2008) 845.
[2] N.A. Khan, S. Shaikhutdinov, H.-J. Freund, Catal. Lett. 108 (2006) 159.
[3] S. Gonzalez, K.M. Neyman, S. Shaikhutdinov, H.-J. Freund, F. Illas, J. Phys. Chem. C 111 (2007) 6852.
[4] F.R. Negreiros, Z. Kuntová, G. Barcaro, G. Rossi, R. Ferrando, A. Fortunelli, J. Chem. Phys. 132 (2010) 234703.
[5] R. Ferrando, A. Fortunelli, R.L. Johnston, Phys. Chem. Chem. Phys. 10 (2008) 640.
[6] G. Rossi, A. Rapallo, C. Mottet, A. Fortunelli, F. Baletto, R. Ferrando, Phys. Rev. Lett. 93 (2004) 105503.
[7] G. Rossi, A. Rapallo, R. Ferrando, A. Fortunelli, B.C. Curley, L.D. Lloyd, R.L. Johnston, J. Chem. Phys. 122 (2005) 194309.
[8] C.R. Henry, Surf. Sci. Rep. 31 (1998) 235.
[9] C.R. Henry, Prog. Surf. Sci. 80 (2005) 92.
[10] P. Guénard, G. Renaud, B. Villette, Phys. B 221 (1996) 205.
[11] J. Goniakowski, Phys. Rev. B 57 (1997) 1935.
[12] I. Yudanov, G. Pacchioni, K. Neyman, N. Rosch, J. Phys. Chem. B 101 (1997) 2786.
[13] N. Lopez, F. Illas, J. Phys. Chem. B 102 (1998) 1430.
[14] A.V. Matveev, K.M. Neyman, I.V. Yudanov, N. Rosch, Surf. Sci. 426 (1999) 123.
[15] O. Robach, G. Renaud, A. Barbier, Phys. Rev. B 60 (1999) 5858.
[16] G. Renaud, A. Barbier, O. Robach, Phys. Rev. B 60 (1999) 5872.
[17] A.M. Ferrari, C.Y. Xiao, K.M. Neyman, G. Pacchioni, N. Rosch, Phys. Chem. Chem. Phys. 1 (1999) 4655.

[18] C.T. Campbell, D.E. Starr, J. Am. Chem. Soc. 124 (2002) 9212.
[19] W. Vervisch, C. Mottet, J. Goniakowski, Phys. Rev. B 65 (2002) 245411.
[20] M. Yulikov, M. Sterrer, M. Heyde, H.-P. Rust, T. Risse, H.-J. Freund, G. Pacchioni, A. Scagnelli, Phys. Rev. Lett. 96 (2006) 146804.
[21] R. Ferrando, G. Rossi, A.C. Levi, Z. Kuntová, F. Nita, G. Barcaro, A. Fortunelli, A. Jelea, C. Mottet, J. Goniakowski, J. Chem. Phys. 130 (2009) 174702.
[22] J. Goniakowski, A. Jelea, C. Mottet, G. Barcaro, A. Fortunelli, Z. Kuntová, F. Nita, A.C. Levi, G. Rossi, R. Ferrando, J. Chem. Phys. 130 (2009) 174703.
[23] C. Revenant, G. Renaud, R. Lazzari, J. Jupille, Nucl. Instrum. Meth. Phys. Res. B 246 (2006) 112.
[24] A.M. Ferrari, C. Xiao, K.M. Neyman, G. Pacchioni, N. Rosch, Phys. Chem. Chem. Phys. 1 (1999) 4655.
[25] J. Oviedo, J.F. Sanz, N. Lopez, F. Illas, J. Phys. Chem. B 104 (2000) 4342.
[26] C. Mottet, J. Goniakowski, F. Baletto, R. Ferrando, G. Tréglia, Phase Transitions 77 (2004) 101.
[27] L. Giordano, G. Pacchioni, Surf. Sci. 575 (2005) 197.
[28] L. Xu, G. Henkelman, C.T. Campbell, H. Jonsson, Phys. Rev. Lett. 95 (2005) 146103.
[29] G. Barcaro, A. Fortunelli, F. Nita, R. Ferrando, Phys. Rev. Lett. 95 (2005) 246103.
[30] G. Barcaro, A. Fortunelli, G. Rossi, F. Nita, R. Ferrando, Phys. Rev. Lett. 98 (2007) 156101.
[31] N.A. Khan, A. Uhl, S. Shaikhutdinov, H.-J. Freund, Surf. Sci. 600 (2006) 1849.
[32] G. Barcaro, A. Fortunelli, J. Phys. Chem. C 111 (2007) 11384.
[33] L.G. Wang, A. Zunger, Phys. Rev. B 67 (2003) 092103.
[34] F. Cyrot-Lackmann, F. Ducastelle, Phys. Rev. B 4 (1971) 2406.
[35] R.P. Gupta, Phys. Rev. B 23 (1981) 6265.
[36] V. Rosato, M. Guillopé, B. Legrand, Phyl. Mag. A 59 (1989) 321.
[37] F. Baletto, R. Ferrando, A. Fortunelli, F. Montalenti, C. Mottet, J. Chem. Phys. 116 (2002) 3856.
[38] F. Cleri, V. Rosato, Phys. Rev. B 48 (1993) 22.
[39] L.O. Paz-Borbón, R.L. Johnston, G. Barcaro, A. Fortunelli, J. Chem. Phys. 128 (2008) 134517.
[40] G. Barcaro, A. Fortunelli, J. Chem. Theory Comput. 1 (2005) 972.
[41] The numerical parameters for the metal-surface interaction can be found in http://www.cinam.univ-mrs.fr/mottet/param/metalMgO.pdf and http://h2.ipcf.cnr.it/alex/webparam.pdf.
[42] J.P.K. Doye, D.J. Wales, J. Phys. Chem. A 101 (1997) 5111.
[43] G. Rossi, R. Ferrando, Chem. Phys. Lett. 423 (2006) 17.
[44] G. Rossi, R. Ferrando, J. Phys. Cond. Mat. 9 (2009) 084208.
[45] D. Faken, H. Jónsson, Comput. Mat. Sci. 2 (1994) 279.
[46] L.O. Paz-Borbon, T.V. Mortimer-Jones, R.L. Johnston, A. Posada-Amarillas, G. Barcaro, A. Fortunelli, Phys. Chem. Chem. Phys. 9 (2007) 5202.
[47] P. Giannozzi, S. Baroni, N. Bonini, M. Calandra, R. Car, C. Cavazzoni, D. Ceresoli, G.L. Chiarotti, M. Cococcioni, I. Dabo, A. Dal Corso, S. de Gironcoli, S. Fabris, G. Fratesi, R. Gebauer, U. Gerstmann, C. Gougoussis, A. Kokalj, M. Lazzeri, L. Martin-Samos, N. Marzari, F. Mauri, R. Mazzarello, S. Paolini, A. Pasquarello, L. Paulatto, C. Sbraccia, S. Scandolo, G. Sclauzero, A.P. Seitsonen, A. Smogunov, P. Umari, R.M. Wentzcovitch, J. Phys. Condens. Matter 21 (2009) 395502.
[48] J.P. Perdew, K. Burke, M. Ernzerhof, Phys. Rev. Lett. 77 (1996) 3865.
[49] D. Vanderbilt, Phys. Rev. B 41 (1990) 7092.The pseudopotentials used in the calculations are Pd.pbe-rrkjus.UPF and Ag.pbe-d-rrkjus.UPF from http://www.quantum-espresso.org.
[50] F. Baletto, C. Mottet, R. Ferrando, Phys. Rev. Lett. 90 (2003) 135504.